Biosensors and Bioelectronics 69 (2015) 280–286

Contents lists available at ScienceDirect

Biosensors and Bioelectronics

journal homepage: www.elsevier.com/locate/bios

A novel amperometric biosensor based on gold nanoparticles anchored on reduced graphene oxide for sensitive detection of L-lactate tumor biomarker

Sawsen Azzouzi [a,b], Lucian Rotariu [a,c], Ana M. Benito [d], Wolfgang K. Maser [d], Mounir Ben Ali [b], Camelia Bala [a,c,*]

[a] LaborQ, University of Bucharest, 4-12 Regina Elisabeta Blvd., 030018 Bucharest, Romania
[b] University of Sousse, Higher Institute of Applied Sciences and Technology of Sousse, 4003 Tunisia
[c] Department of Analytical Chemistry, University of Bucharest, 4-12 Regina Elisabeta Blvd., 030018 Bucharest, Romania
[d] Instituto de Carboquímica ICB-CSIC, C/Miguel Luesma Castán 4, 50018 Zaragoza, Spain

ARTICLE INFO

Article history:
Received 19 December 2014
Received in revised form
4 March 2015
Accepted 5 March 2015
Available online 7 March 2015

Keywords:
Reduced graphene oxide
Gold nanoparticles
NADH
L-lactate
Cancer biomarker
L-lactate dehydrogenase

ABSTRACT

In this work, a novel amperometric biosensor based on gold nanoparticles anchored on reduced graphene oxide (RGO-AuNPs) and L-lactate dehydrogenase (LDH) was developed for the sensing of L-lactate. Firstly, the RGO-AuNPs modified screen printed electrodes were tested for NADH detection showing a wide dynamic range and a low detection limit. Next, the biosensor was constructed by incorporating both enzyme and RGO-AuNPs in a sol gel matrix derived from tetrametoxysilane and methyltrimetoxysilane. The enzyme loading, working pH, and coenzyme concentration were optimized. The biosensor linearly responded to L-lactate in the range of 10 μM–5 mM and showed a good specific sensitivity of 154 μA/mM cm^2 with a detection limit of 0.13 μM. This was accompanied by good reproducibility and operational stability. Tests on artificial serum proved that L-lactate can be determined practically without interferences from commonly interfering compounds such as urate, paracetamol and L-ascorbate. Our LDH/RGO-AuNPs/SPCE based biosensor thus performs as electrochemical device for the detection of L-lactate as a viable early cancer bio-marker.

1. Introduction

Malignant transformation of normal cells into tumor cells very frequently leads to an increased accumulation of lactate concentration in most solid tumors (Hirschhaeuser et al., 2011), as it has been reported in clinical studies on prostate and breast cancer (Lupo et al., 2010; Tessem et al., 2008). This characteristic renders L-lactate a viable early cancer bio-marker. Pathophysiologic accumulation of L-lactate has been also associated with a high risk for the formation of metastases and thus with overall low survival chances of cancer patients. Tumor metabolism by releasing a high amount of lactate to the extracellular space largely contributes to the immunologic escape. Leukocytes may be asphyxiated by the presence of lactate. The differentiation of monocytes to dendritic cells is inhibited by lactate and cytokine release from dendritic cells (Gottfried et al., 2006) and cytotoxic T cells (Fischer et al., 2007) are inactivated. Thus is becomes clear that monitoring of the L-lactate concentration is important not only for the detection of cancer in its early stage but also during the antitumoral treatment.

The development of methods for L-lactate detection has gained considerable attention in clinical diagnostics, food analysis, biotechnology and sports medicine (Palleschi et al., 1990; Sartain et al., 2006). Moreover, many methods have been reported for lactate determination, such as chromatographic and spectrometric analysis (Bariskaner et al., 2003; Wulkan et al., 2001). However, these methods are time consuming, complex to perform, expensive and require laborious sample pretreatment. Thus, there is a considerable need for the development of inexpensive, rapid and reliable methods for lactate quantification. In this sense, electrochemical sensors, specially employing sensitive enzyme-based amperometric biosensors, offer a cost-effective solution to achieve fast response and high sensitivity (Li et al., 2012).

The enzymes normally used in the development of amperometric biosensors for L-lactate detection (Ibupoto et al., 2012) are lactate oxidase (LOD) (Hirano et al., 2002; Spohn et al., 1996) and

* Corresponding author at: Department of Analytical Chemistry, University of Bucharest, 4-12 Regina Elisabeta Blvd., 030018 Bucharest, Romania.
Fax: +40 21 4104888.
E-mail address: camelia.bala@g.unibuc.ro (C. Bala).

http://dx.doi.org/10.1016/j.bios.2015.03.012
0956-5663/

L-lactate dehydrogenase (LDH) (Chaubey et al., 2000; Leonida et al., 2003). The most commonly used lactate biosensor reported in the literature is based on the specific recognition of L-lactate using LDH. The LDH enzyme catalyzes the oxidation of lactate in the presence of nicotinamide adenine dinucleotide (NAD^+). to pyruvate and reduced form of nicotinamide adenine dinucleotide (NADH), which can be detected amperometrically (Pereira et al., 2007). This enzyme has some important advantages for monitoring the L-lactate in real samples. Among others, it overcomes the problem of oxygen dependency, and offers a high selectivity for L-lactate compared to LOD. Enzymatic amperometric sensors based on L-lactate dehydrogenase (LDH) are presented as an attractive approach for detection of L-lactate in biological samples (Rassaei et al., 2013) due to their simple design and good performances. However, the LDH based biosensor has some drawbacks, including the low stability of the enzyme and the electrochemical oxidation of NADH that occurs at high over potentials (Santos et al., 2002).

The main problem of the direct detection of NADH in biological samples is the interference from electroactive species such as ascorbic acid, paracetamol, uric acid, which undergo redox reactions at relatively low applied potential and thus reduce the selectivity of the biosensor. Different approaches that include the use of electron mediators (Prieto-Simón and Fàbregas, 2004), carbon nanotubes (Musameh et al., 2002; Pereira et al., 2007; Saleh et al., 2011a), conducting polymers (Chaubey et al., 2000; Rahman et al., 2009; Saleh et al., 2011b), chitosan composites (Ge et al., 2009), polyelectrolytes (Rotariu et al., 2014) were reported to improve the sensitivity and selectivity of the LDH biosensors.

Due to their large surface, excellent electrical conductivity and chemical stability, graphene based materials were lately used for many electrochemical application that includes detection of NADH (Gasnier et al., 2013; Guo et al., 2011; Kuila et al., 2011). Multiple possibilities of graphene functionalization have considerably enhanced the field of biosensing applications.

In the present work, a novel amperometric biosensor based on gold nanoparticles anchored on reduced graphene oxide (RGO-AuNPs) and L-lactate dehydrogenase (LDH) was developed for the sensing of L-lactate. In the first step, the RGO-AuNPs modified screen printed electrodes were tested for NADH detection showing a large linear range and a low limit of detection. Then, the biosensor was developed by incorporating both enzyme and RGO-AuNPs in a sol gel matrix derived from tetrametoxysilane and methyltrimetoxysilane. A scheme describing the working principle of the LDH/RGO-AuNPs/SPCE biosensor can be found in Fig. 1. The common interfering electroactive compounds such as ascorbic acid, uric acid and paracetamol have been studied.

2. Materials and methods

2.1. Materials

Graphite powder, sulfuric acid (H_2SO_4), sodium nitride ($NaNO_3$), potassium permanganate ($KMnO_4$), sodium citrate, tetrachloroauric (III) acid ($HAuCl_4$), sodium borohydride ($NaBH_4$), nicotinamide adenine dinucleotide reduced disodium salt (NADH) and NAD+, potassium ferricyanide ($K_3[Fe(CN)_6]$), potassium ferrocyanide ($K_4[Fe(CN)_6]$) were obtained from Sigma-Aldrich and used without further purification. Tetramethoxysilane (TMOS), methyltrimethoxysilane (MTMOS), polyethylene glycol (PEG600) were purchased from Fluka. All other chemicals used were of analytical grade. Phosphate buffer solution (PBS, 0.1 M, containing 0.1 M KCl, pH=7.5) was prepared by mixing solution of Na_2HPO_4, NaH_2PO_4 and KCl. All solutions were prepared in ultrapure water (Millipore, 18 MΩ cm).

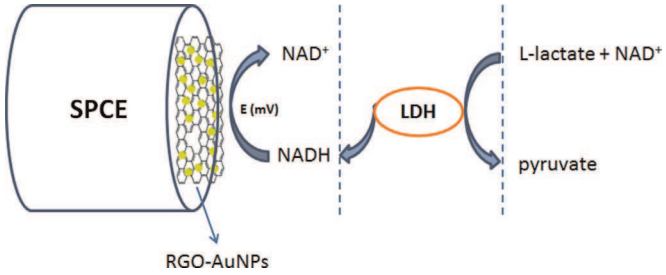

Fig. 1. Schematic representation of working principle of the LDH/RGO-AuNPs/SPCE biosensor.

2.2. Instrumentation

The metal loading in the graphene was determined by inductive Coupled Plasma Spectroscopy (ICPS), using a Jobin-Yvon 2000 Ultrace Analyzer. Size and distribution of Au nanoparticles were studied by transmission electron microscopy (TEM), using a JEOL-2000 FXII equipment working at 200 kV. X-ray photoelectron spectroscopy (XPS) was carried out on an ESCAPlus Omicron spectrometer using a monochromatized Mg X-ray source (1253.6 eV). Data were analyzed using Casa XPS software package.

Cyclic voltammetry (CV) and amperometric measurements were performed using a computer-controlled μ-Autolab type III and electrochemical impedance spectroscopy (EIS) experiments with an Autolab PGSTAT 101. Nova 1.10 software was used to gather data. The screen-printed carbon electrodes (SPCE, Dropsens DRP-110) consisted of a three-electrode system having a carbon working electrode (4 mm diameter), an Ag pseudo-reference electrode and a carbon counter electrode. All potentials are reported vs. Ag pseudo-reference electrode and all experiments were carried out at room temperature (22 °C), using a 5 mL cell.

2.3. Thermal exfoliation/reduction of graphite oxide

Graphite oxide was first prepared using a modified Hummer's method from graphite powder by oxidation with $NaNO_3$, H_2SO_4 and $KMnO_4$ in an ice bath as reported elsewhere (Hummers and Offeman, 1958; Vallés et al., 2012). In brief, 170 mL of concentrated H_2SO_4 was added to a mixture of graphite flakes (5.0 g) and $NaNO_3$ (3.75 g), and the mixture was cooled in an ice bath, and stirred for thirty minutes. $KMnO_4$ (25 g) was slowly added and stirred for another thirty minutes. The reaction was then warmed to 35 °C, and stirred for two more hours. Water (250 mL) was slowly added, and then 30% H_2O_2 (20 mL). The mixture was stirred for an hour, filtered, and the obtained powder was repeatedly washed with 400 mL of HCl:H_2O (1:10), and dried. Next, 300 mg of the synthesized graphite oxide was heated at 700 °C for 15 min under Ar atmosphere affording the graphene-like material (RGO).

2.4. Synthesis of hybrid material RGO-AuNPs

In a typical experiment, 5.8 μmol of sodium citrate were added to 20 mL $HAuCl_4$ aqueous solution (5.2×10^{-5} M). The mixture was stirred at room temperature until clear solution is observed. Then, 70 μL of freshly prepared cold (0 °C) $NaBH_4$ in water (0.1 M) were added dropwise. Next, 10 mg of thermally exfoliated graphene (RGO) were added, and the mixture stirred at room temperature until a complete loss of color was observed (60 min). Finally, the dispersion was vacuum filtered, washed with distilled water (300 mL), and dried overnight at 80 °C.

2.5. Modification of the screen-printed electrodes

We have dispersed 0.5 mg of RGO-AuNPs in 1 mL water to form 0.5 mg/mL RGO-AuNPs suspension under stirring and sonication

for 1 h. The obtained RGO-AuNPs suspension was stored for 24 h at 4 °C. Prior to modification, the SPCEs were electrochemically pretreated by cycling the potential between −0.5 and 0.5 V in PBS (0.1 M containing 0.1 M KCl, pH=7.5) until a reproducible shape of the voltammogram was obtained. Then, 5 μL of the RGO-AuNPs suspension (0.5 mg/mL) was deposited on the surface of working electrode and then was left to dry, at 4 °C in a desiccator, for 24 h.

2.6. Preparation of L-lactate biosensor

An important area of biosensor research is the immobilization of enzymes at transducer surfaces. The sol gel matrix was prepared according to the method reported earlier (Rotariu et al., 2012). 5 μL of TMOS was mixed with 15 μL MTMOS, 40 μL HCl (1 mM), 44 μL and 4 μL PEG 600. The mixture was sonicated for about 15 min and then kept at 4 °C for hydrolysis for about 6 h. Then, we mixed the prepared sol–gel with L-lactate dehydrogenase solution in ratio 30:70 (v/v). An appropriate volume (500 μL) of RGO-AuNPs suspension (0.5 mg/mL) was added to the mixture under stirring and finally, 10 μL dropped on the surface of the working electrode in order to obtain 3.8 IU/electrode. Subsequently, the biosensor was left to dry for two days in a desiccator at 4 °C.

3. Results and discussion

3.1. RGO-AuNPs characterization

Fig. 2A shows TEM images of a flake of the parent RGO material and the final RGO-AuNPs hybrid material. The parent RGO flakes reveal lateral sizes in the range of a few micrometers (image a). The surface of the parent RGO flakes is homogeneously covered by small gold nanoparticles (AuNPs) with diameters ranging from 2 to 6 nm (images b, c). According to ICPS analysis, the overall Au loading amounts to 2 wt% corresponding to a deposition yield of 98%.

High resolution XPS scan from the carbon (C1s) region (Fig. 2B graph a) allow to identify oxygen-containing groups, and to quantify the oxygen content in the RGO-AuNPs hybrid material. Deconvolution of the C1s signal revealed the presence of a main peak at 284.3 eV, corresponding to graphitic carbon, together with additional contributions assigned to non-conjugated carbon (285.1 eV), C–O in phenols, ethers and hydroxyls (285.8 eV), *C*=O in carbonyl or quinones (286.9 eV), *O*=C–O in carboxyls, carboxylic anhydrides, and esters (288.8 eV), and the characteristic shakeup line of carbon in aromatic compounds at 290.3 eV (π–π* transition) (Figueiredo and Pereira, 2010). Analysis of the XPS C1 survey spectra provided an overall oxygen content of 4 at% in the RGO-AuNPs hybrid material. In addition, the XPS scan of the Au 4f orbital clearly reveals the presence of gold in the samples (Fig. 2B graph b).

3.2. Electrochemical oxidation of NADH

3.2.1. Cyclic voltammetry studies

The bare SPCE and RGO-AuNPs modified electrodes were tested in the presence and in the absence of NADH 5 mM solutions by cyclic voltammetry. No oxidation peak was observed for both types of electrodes in the absence of NADH (Fig. 3A a, b). The CV response of bare SPCE displays in the presence of NADH an oxidation peak at +0.6 V (Fig. 3A c). However, as it can be seen in Fig. 3A d, the RGO-AuNPs modified electrode reveals an oxidation

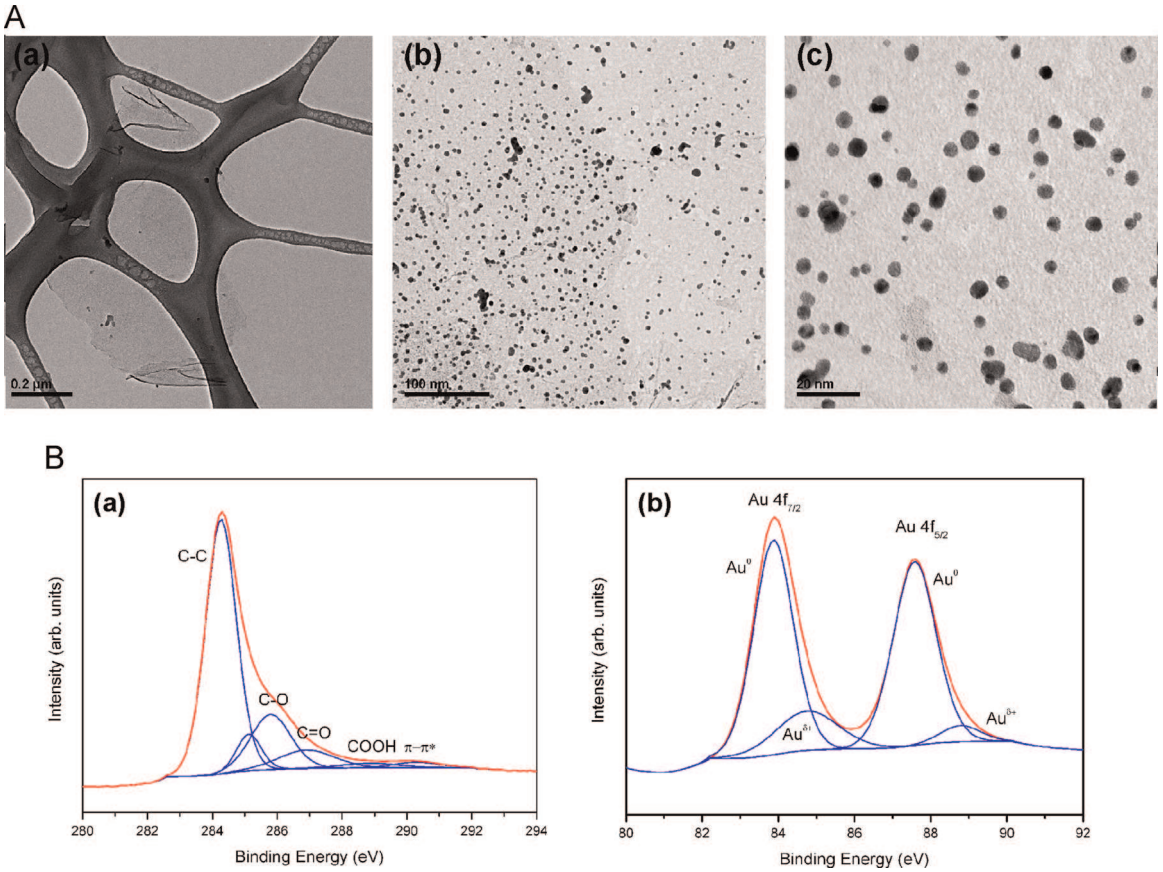

Fig. 2. (A) TEM images of (a) a flake of the starting RGO material, and the RGO-AuNPs hybrid material at (b) low magnification and (c) high magnification. (B) Characterization of RGO-AuNPs: (a) XPS spectra of C1s orbitals of the RGO-Au hybrid material, (b) XPS spectra of Au $4f_{7/2}$ and Au $4f_{5/2}$ orbitals of the RGO-Au hybrid material.

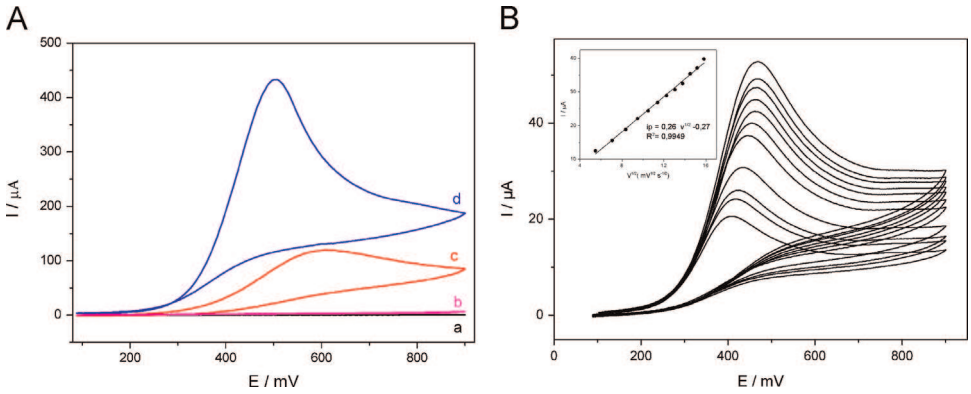

Fig. 3. (A) Cyclic voltammograms recorded in PBS for bare electrode (a) and RGO-AuNPS/SPCE (b) and in 5 mM NADH for bare electrode (c) and RGO-AuNPS/SPCE (d) (SR=100 mV/s, pH=7.5). (B) Cyclic voltammograms of RGO-AuNPs/SPCE recorded in 1 mM NADH for different scan rate. Inset-influence of the scan rate on the peak current (SR=30–250 mV/s, pH=7.5).

peak of NADH at +0.48 V. We also noticed a significant increase of the oxidation current from 73 µA for the bare electrode to 350 µA in the presence of the RGO-AuNPs layer. This behavior can be explained by taking into consideration the nature of the materials used for the modification of the working electrode and the existence of a synergistic effect of the precursors. Firstly, the conjugated surface structure of graphene with its unique electronic properties facilitates fast electron transfer processes. Secondly, the presence of AuNPs, in addition to its well-known electrocatalytical properties, leads to an increase of the active surface. The excellent electrocatalytical properties of RGO-AuNPs is reflected by a significant increase of the NADH oxidation current and a shifting of the peak potential toward lower oxidation potential compared with the unmodified electrode.

Cyclic voltammograms recorded in 1 mM NADH at scan rates ranging from 30 to 250 mV/s are presented in Fig. 3B. It can be clearly seen that the oxidation peak currents i_p increase linearly with the square root of the scan rate (see inset Fig. 3B.) suggesting that the reaction is controlled by diffusion process (Nicholson and Shain, 1964).

3.2.2. Effect of RGO-AuNPs amount on the sensor response

The concentration of the RGO-AuNPs suspension can affect the sensor response to NADH. In order to study this effect, we have deposited aliquots of RGO-AuNPs suspension of different concentrations on the surface of working electrode and let it to dry according to the procedure described above. The SPCE sensors were tested by cyclic voltammetry and the peak currents for NADH 1 mM were compared. We have recorded the highest current for a RGO-AuNPs concentration of 0.5 mg/mL. At lower concentrations of RGO-AuNPs, a low response and unstable RGO-AuNPs films were obtained. The signal was lower for higher concentrations of RGO-AuNPs. Apparently, beyond a critical amount of RGO-AuNP diffusion processes are hindered and limit the sensor response.

3.2.3. Electrochemical impedance spectroscopy studies

Nyquist profiles obtained for bare electrode, RGO-AuNPs and LDH/RGO-AuNPs electrodes in 5 mM $Fe(CN)_6^{3-/4-}$ containing 0.1 M KCl are presented in the Supporting information (Fig. S1). These are characterized by a semicircular portion followed by a linear part at lower frequencies. This linear part could be attributed to the diffusion of redox species. Modeling of the impedance data was realized according to Randles circuit, depicted in the inset of Fig. S1. It is based on the charge transfer resistance (R_{ct}), the constant phase element (CPE), the solution resistance (R_s), and the Warburg impedance (W).

The resistance of charge transfer for bare SPCE and RGO-AuNPs/SPCE was found to be 5.39 kΩ, and 1.23 kΩ, respectively. It becomes obvious that the higher conductivity of RGO-AuNPs/SPCE facilitates the charge transfer. When LDH was introduced in the nanocomposite structure by sol–gel entrapment, the value of the electron transfer resistance increased to 3.14 kΩ. This observation could be attributed either to the sol–gel matrix acting, as barrier, which hinders the efficient interfacial charge transfer, or to the macromolecular structure of LDH, which blocks the $Fe(CN)_6^{3-/4-}$ redox species. These results prove that the charge transfer is favored by the presence of the nanocomposite layer consisting of reduced graphene oxide and gold nanoparticles, due to the electrostatic interaction between positively charged electrode surface and negatively charged redox species $Fe(CN)_6^{3-/4-}$.

3.2.4. Chronoamperometric measurements

Chronoamperometric experiments on modified electrode with RGO-AuNPs were performed using phosphate buffer solution and different concentrations of NADH and are shown in the Supporting information (Fig. S2). The working electrode was polarized at +480 mV vs. Ag/AgCl. Fig. S2A shows the chronoamperograms and experimental data involved in determining the catalytic rate constant k_{cat} according to the following equation:

$$\frac{i_{cat}}{i_{buffer}} = \pi^{1/2} (k_{cat} C t)^{1/2} \quad (1)$$

Here i_{cat} and i_{buffer} are the currents in the presence and in the absence of NADH, C represents the NADH concentration and t is the time in second. Plotting i_{cat}/i_{buffer} vs. $t^{1/2}$ for 5 mM NADH reveals a linear dependence (inset Fig. S2A) whose slope was used to calculate a rate constant of 4.38×10^5 M^{-1} s^{-1}. This value is higher than the ones obtained by other types of electrodes for NADH detection and thus clearly indicates that RGO-AuNPs film is suitable for developing NADH sensors. For example, a value of 1.5×10^4 M^{-1} s^{-1} was calculated using chronoamperometric data and SPCE electrode modified with SWCNT-COOH and variamine (Radoi et al., 2008). Moreover, by using poly(allylamine hydrochloride) modified SPCE, a value of 9.38×10^4 M^{-1} s^{-1} was reported (Rotariu et al., 2014). Also, using hydrodynamic voltammetry on poly(phenosafranin)-modified carbon electrodes, a maximum value of the catalytic constant of 1.6×10^4 M^{-1} s^{-1} was mentioned (Saleh et al., 2011b). A value of 3.36×10^5 M^{-1} s^{-1} was obtained for a modified electrode with composite material based on poly(phenosafranin) functionalized single-walled carbon nanotubes (Saleh et al., 2011a).

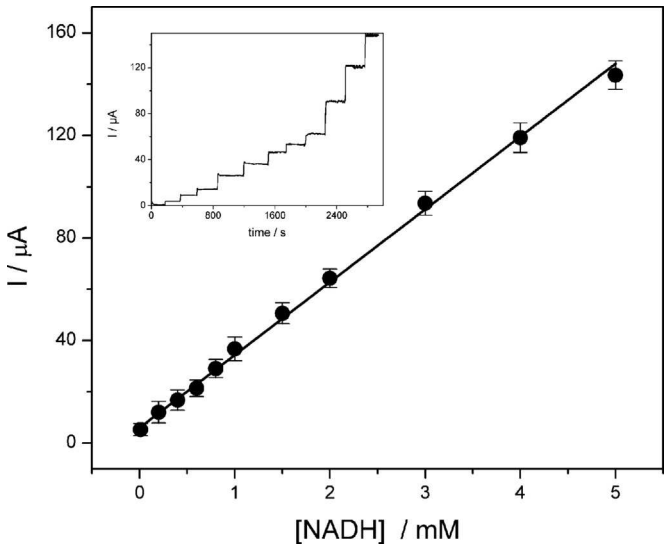

Fig. 4. Calibration plot for NADH using RGO-AuNPs /SPCE ($n=3$). Inset: typical current–time response curves for NADH ($E=+480$ mV, pH=7.5).

Chronoamperometric measurements were used also to estimate the NADH diffusion coefficient (D) based on Cottrel equation [24]:

$$I = \frac{nFAD^{(1/2)}\,C}{\pi^{(1/2)}\,t^{(1/2)}} \qquad (2)$$

The linear parts of the I vs. $t^{1/2}$ plots were utilized to estimate the slope for each NADH concentration (Fig. S2B). The diffusion coefficient of 1.6×10^{-5} cm^2 s^{-1} was determined from the plot ($I\cdot t^{1/2}$) vs. NADH concentration. This value is higher than other diffusion coefficients reported in literature. For instance, a value of 1.15×10^{-7} cm^2 s^{-1} was obtained for a poly(allylamine hydrochloride) modified SPCE (Rotariu et al., 2014).

3.2.5. Calibration of RGO-AuNPs/SPCE sensor

The analytical performances of the RGO-AuNPs modified SPC electrodes towards the detection of NADH has been tested using amperometry. The potential of the electrode was held at +480 mV and aliquots of NADH were injected at regular interval of time into the stirred supporting electrolyte solution. A typical response for NADH is presented as inset in Fig. 4.

The calibration graph was performed, for NADH concentrations in the range of 0.01–5 mM (Fig. 4). A fast and stable response of the sensor was observed. For all the concentrations tested, the 95% of steady state current value was achieved within 6 s. The sensitivity and limit of detection (based on signal to noise ratio of 3) were calculated to be 226.1 ± 3.3 µA/mM cm^2 (RSD=1.47%) and 0.1 µM respectively. At higher concentration, the current response decreased and the signal to noise ratio became larger. This can be attributed to the restrictions of NADH diffusion at this concentration range. A very high sensitivity was achieved for NADH detection using RGO-AuNPs/SPCE compared to only 27.07 µA/mM cm^2 for an GC electrode modified with RGO-Au nanorods (Li et al., 2013) or to 178.3 µA/mM cm^2 for RGO/GC electrode (Guo et al., 2011). The detection limit was also within one and two order of magnitude lower with respect to these graphene based sensors.

The stability of the modified electrodes was examined in the presence of NADH for 10 min under stirring condition by amperometric measurements. Remarkably, a current decrease of only 7% was observed upon stirring. This fact clearly highlights the high operational stability of the RGO-AuNPs modified electrode and further confirms its suitability for biosensing applications.

3.3. Amperometric L-lactate biosensor

NADH sensor provides a sensitive and selective platform for developing a LDH based biosensor for L-lactate detection. Due to the low stability of the LDH enzyme the immobilization of LDH is crucial for the performances of the L-lactate biosensor. Sol–gel matrices are highly suitable when it comes to the use of sensitive enzymes (Rotariu et al., 2012). Moreover, mixing the sol–gel with the RGO/AuNPs allows an intimate contact between enzyme and electroactive material leading to a highly responsive system in terms of a fast electron transfer and a short response time.

3.3.1. Optimization of the working potential

The preparation procedure of the L-lactate biosensor, which requires mixing of RGO-AuNPs with LDH in a sol–gel followed by a further deposition on the SPCE leads to a modification of the NADH electrochemical transducer properties. Therefore, the most suitable potential for amperometric detection of NADH produced in the enzymatic reaction needs to be analyzed first for the LDH/RGO-AuNPs modified biosensor. For this purpose, we have performed calibration of the L-lactate biosensor at pH=7.5 and different working potentials. The concentration of NAD^+ was kept at 3 mM. The obtained sensitivities were plotted against the applied potentials and are shown in Fig. 5A. While the response below +300 mV is rather low, a significant increase is observed from +300 mV to +500 mV. Based on these data, we have chosen +480 mV vs. Ag/AgCl as an operating potential in order to obtain a signal with good intensity and fast response while avoi-ding interference from several other compounds. This value was used for

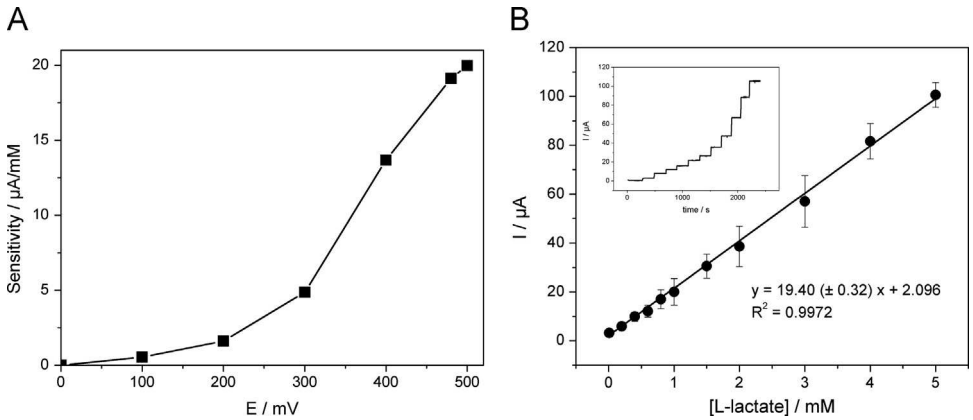

Fig. 5. A) L-Lactate response of the LDH/RGO-AuNPs/SPCE to different applied potentials ([NAD^+]=3 mM, pH=7.5). (B) Calibration graph for L-lactate using LDH/RGO-AuNPs/SPCE ($n=3$). Inset: typical current–time response curves for L-lactate ($E=+480$ mV, [NAD^+]=3 mM, pH=7.5).

all the subsequent amperometric measurements.

3.3.2. Effect of enzyme loading

The amperometric response of the L-lactate biosensor depends on LDH loading. For this reason we have prepared several biosensors using different sol–gel:enzyme ratio (vol). Highest sensitivities were achieved using 70 μL of LDH solution and 30 μL sol–gel (3.8 IU on the working electrode). This enzyme loading was used for all further experiments.

3.3.3. Effect of pH

The enzyme activity depends on the pH of supporting electrolyte and the enzyme immobilization methodology. The effect of the pH on the LDH/RGO-AuNPs/SPCE biosensor's response to L-lactate was studied in the pH range between 6 and 8.5 in order to promote the reaction in the direction of L-lactate oxidation. Biosensor calibration was performed in the linear range from 10 μM to 3 mM in the presence of 3 mM NAD^+. A significant increase of the sensitivity from 59 to 160 μA/mM cm^2 was observed from pH 6 to pH 7.5.

Our results reveal that the biosensor exhibits a good response in the pH range of 7–8. The response decreases for pH value higher than 8.0 or lower than 7.0, and a maximum response is obtained at about pH 7.5. Hence, we have selected a pH of 7.5 for all further studies.

3.3.4. Effect of coenzyme concentration

The concentration of NAD^+ has been investigated in order to find the optimal concentration which must be used to have the best response of L-lactate biosensor. In this context, we have calibrated L-lactate biosensor using different concentration of NAD^+ in the range from 1 to 5 mM at an applied potential of +480 mV and pH 7.5.

The sensitivity increases with increasing the concentration of NAD^+ and reaches a maximum at 3 mM. For concentrations higher than 3 mM, we observe a significant decrease of the sensitivity. This can be due to the inhibitory effect of LDH activity due to the excess of substrate (Jena and Raj, 2007). 3 mM NAD^+ was used in all further experiments.

3.3.5. Biosensor calibration for L-lactate

We have calibrated L-lactate biosensor at a pH 7.5 and a fixed concentration of 3 mM NAD^+. The potential of the electrode was held at +480 mV and aliquots of L-lactate were injected at regular interval of time into the stirred supporting electrolyte solution.

The calibration graph shown in Fig. 5B was obtained, for a lactate concentration range of 0.01–5 mM. A fast and stable response of the sensor was observed. A response time of 8 s for the entire range of concentrations was attained. The values for the sensitivity and limit of detection (based on signal to noise ratio of 3) amount to 154.4 ± 2.5 μA/mM cm^2 (RSD = 1.60%) and 0.13 μM, respectively. A comparison with available data from literature for other types of L-lactate biosensors is presented in the Supporting information (Table S1). Unfortunately the specific sensitivity is not always reported thus impeding a direct comparison in some of the cases. Nevertheless, it clearly can be seen that the LDH/RGO-AuNPs based biosensor presented in this work exhibits, with more than 3 decades of concentration, one of the largest response ranges, in addition to a low limit of detection. Moreover, the linear response of our biosensor covers the entire range of L-lactate concentrations in serum for both normal and cancer biomarker levels, and thus ones more underlines its importance for practical applications.

3.3.6. Stability and reproducibility of the biosensor

The planar characteristics of the sensors produced by screen printed technique usually require a good and reproducible contact between transducer and enzymatic layer.

Operational stability was estimated by measuring the sensors response to 10 μM lactate in 0.1 M phosphate buffer (pH = 7.5) containing 3 mM NAD^+ with intermediate rinsing of the cell, at an applied potential of +480 mV vs. Ag/AgCl. We have achieved good stabilities, for 20 successive injections and have obtained an average current of 3.17 ± 0.05 μA. The relative standard deviation for a series of twenty successive measurements was 1.57%.

Storage stability was estimated by carrying out a calibration of the biosensor every 2 days, the electrodes being stored in a desiccator at 4 °C when not in use. The biosensor sensitivity was compared during the test period.

A slight increase of the sensitivity was observed in the first days. After 7 days, the LDH sol–gel based biosensor exhibited an enhancement of 8% with respect to its response at the first day. Afterwards, the response remained stable for the next 25 days. After this period, a decrease on the sensor sensitivity was observed. The good stability of the sensor response easily competes with other L-lactate biosensors. For instance, a stability of 14 days using polypyrrole–polyvinyl sulfonate interface has been reported (Chaubey et al., 2000). A L-lactate biosensor based on LDH/ZnO nanorods was stable for only 23 days (Nesakumar et al., 2014). However, a considerable higher value (40 days) was obtained using polyvinylpyrrolidone interface (Yoon and Kim, 1996).

The reproducibility of the biosensor has been investigated using three different electrodes. The relative standard deviation for three individual sensors was 2.5%. Thus, the response of the L-lactate biosensor was considered to be reproducible.

3.3.7. Selectivity of the biosensor

We have been investigated the response of LDH/RGO-AuNPs based biosensor with respect to interfering species commonly found in biological samples. Moreover, we have examined the biosensor response towards 10 μM L-lactate, L-ascorbate, urate and paracetamol individually. The measured current illustrated in Table 1 is the average of three different measurements.

Selective properties of LDH/RGO-AuNPs based L-lactate biosensor were studied using electrochemical amperometric measurements. The addition of L-lactate leads to a well-defined response; however, the successive addition of interfering species such as urate and paracetamol did not lead to a discernable current response. On the other hand, L-ascorbate was found to produce a small current at the same level of concentration with L-lactate. In real serum samples, in the normal therapeutic range, the L-ascorbate is found in a concentration of about 10 times lower than L-lactate. Under these conditions, it is expected to have no interference of ascorbic acid for detection of L-lactate in serum samples.

3.4. Detection of L-lactate in artificial serum

The goal of the present work was the development of a biosensor for the detection, in human serum, of L-lactate that can be considered as a tumor biomarker. Therefore, in order to estimate the response of LDH/RGO-AuNPs based L-lactate biosensor in a real

Table 1
The response of LDH-RGO-AuNPs based biosensor towards lactate and its interfering species.

	L-Lactate 10 μM	L-Ascorbate 10 μM	Urate 10 μM	Paracetamol 10 μM
Current[a] (μA)	3.17 ± 0.05	0.85 ± 0.07	0.19 ± 0.03	not detected
Relative response (%)	100	27	6	0

[a] (n = 3).

sample, we have prepared an artificial serum containing the most common compounds of the real serum with its corresponding concentrations. The normal L-lactate concentration in human serum ranges between 0.5 mM and 1.5 mM (Rassaei et al., 2013). The normal therapeutic range of L-ascorbate is between 0.03 mM and 0.11 mM. Therefore, taking also into consideration the increase of the L-lactate concentration in the case of a cancer tumor, the ratio of [L-lactate]/[L-ascorbate] is higher than 10.

The artificial serum was prepared using the following composition (Merzouk et al., 2014): 8 mmol/L NaH_2PO_4; 1.5 mmol/L Na_2HPO_4; 2.0 mmol/L $CaCl_2$; 0.8 mmol/L $MgCl_2$; 4.5 mmol/L KCl; 0.05 mmol/L NH_4Cl; 4.7 mmol/L glucose; 2.5 mmol/L urea and 0.5 mmol/L urate.

Next, we have measured the current in presence and in absence of 0.1 mM ascorbic acid in the artificial serum after adding for 1 mM L- lactate. After three individual measurements the current decreased from 17.87 ± 0.94 μA in absence of ascorbic acid to 17.37 ± 0.53 μA in presence of 0.1 mM ascorbic acid. However, this decrease falls well within the limits of experimental error. It thus can be concluded that the detection of L-lactate in serum samples by LDH/RGO-AuNPs/SPCE is not affected by the presence of ascorbic acid and uric acid at physiological level. The biosensor we have developed in this work can be successfully used for detection of L-lactate as tumor biomarker in biological samples.

4. Conclusions

A L-lactate dehydrogenase based biosensor using gold nanoparticles anchored on reduced graphene oxide has been developed and characterized. The biosensor response is based on the electrocatalytic detection of enzymatically generated NADH by the RGO-AuNPs layer. First, the RGO-AuNPs layer has shown good sensitivity towards NADH. Next, both LDH and RGO-AuNPs have been incorporated in a sol–gel matrix in order to develop the L-lactate biosensor. Operational parameters of the L-lactate biosensors such as enzyme loading, pH and coenzyme concentration were optimized. Calibration of the biosensors was performed at an applied potential of +480 mV, pH 7.5 using a NAD^+ concentration of 3 mM NAD^+. The LDH/RGO-AuNPs/SPCE based biosensor is highly sensitive towards L-lactate. With a linear response range of more than 3 decades of concentration, it covers the entire concentration range for normal and pathological L-lactate levels, while offering a low limit of detection of 0.13 μM. A high stability of the sensor response of 25 days was achieved. Tests on artificial serum proved that L-lactate can be determined practically without interferences from urate, paracetamol and L-ascorbate. The performances render our LDH/RGO-AuNPs/SPCE biosensor, as a very attractive electrochemical device for early cancer bio-marker detection.

Acknowledgments

This work was supported by Romanian National Authority for Scientific Research (Grant PN-II-ID-PCE-2011-3-0286) and REA-FP7 Marie Curie (Grant PIRSES_GA_2012-318053:SMARTCANCER-SENS). Ana M. Benito and Wolfgang K. Maser would like to thank the Spanish Ministry MINECO (Projects MAT2010-15026 and ENE2013-48816-C5-5-R), the Spanish National Research Council CSIC (Project 201080E124), and the regional Government of Aragon and the European Social Fund (Project DGA-ESF T66) for financial support.

Appendix A. Supplementary material

Supplementary data associated with this article can be found in the online version at http://dx.doi.org/10.1016/j.bios.2015.03.012.

References

Bariskaner, H., Ustun, M.E., Ak, A., Yosunkaya, A., Dogan, N., Gurbilek, M., 2003. Methods Find. Exp. Clin. 25 (5), 371–376.
Chaubey, A., Gerard, M., Singhal, R., Singh, V.S., Malhotra, B.D., 2000. Electrochim. Acta 46 (5), 723–729.
Figueiredo, J.L., Pereira, M.F.R., 2010. Catal. Today 150 (1–2), 2–7.
Fischer, K., Hoffmann, P., Voelkl, S., Meidenbauer, N., Ammer, J., Edinger, M., Gottfried, E., Schwarz, S., Rothe, G., Hoves, S., Renner, K., Timischl, B., Mackensen, A., Kunz-Schughart, L., Andreesen, R., Krause, S.W., Kreutz, M., 2007. Blood 109 (9), 3812–3819.
Gasnier, A., Pedano, M.L., Rubianes, M.D., Rivas, G.A., 2013. Sens. Actuators B 176, 921–926.
Ge, B., Tan, Y., Xie, Q., Ma, M., Yao, S., 2009. Sens. Actuators B 137 (2), 547–554.
Gottfried, E., Kunz-Schughart, L.A., Ebner, S., Mueller-Klieser, W., Hoves, S., Andreesen, R., Mackensen, A., Kreutz, M., 2006. Blood 107 (5), 2013–2021.
Guo, K., Qian, K., Zhang, S., Kong, J., Yu, C., Liu, B., 2011. Talanta 85 (2), 1174–1179.
Hirano, K., Yamato, H., Kunimoto, K., Ohwa, M., 2002. Biosens. Bioelectron. 17 (4), 315–322.
Hirschhaeuser, F., Sattler, U.G.A., Mueller-Klieser, W., 2011. Cancer Res. 71 (22), 6921–6925.
Hummers, W.S., Offeman, R.E., 1958. J. Am. Chem. Soc. 80 (6) 1339-1339.
Ibupoto, Z.H., Shah, S.M.U.A., Khun, K., Willander, M., 2012. Sensors 12 (3), 2456–2466.
Jena, B.K., Raj, C.R., 2007. Electroanalysis 19 (7–8), 816–822.
Kuila, T., Bose, S., Khanra, P., Mishra, A.K., Kim, N.H., Lee, J.H., 2011. Biosens. Bioelectron. 26 (12), 4637–4648.
Leonida, M.D., Starczynowski, D.T., Waldman, R., Aurian-Blajeni, B., 2003. Anal. Bioanal. Chem. 376 (6), 832–837.
Li, J., Li, S., Yang, C.F., 2012. Electroanalysis 24 (12), 2213–2229.
Li, L., Lu, H., Deng, L., 2013. Talanta 113, 1–6.
Lupo, J.M., Chen, A.P., Zierhut, M.L., Bok, R.A., Cunningham, C.H., Kurhanewicz, J., Vigneron, D.B., Nelson, S.J., 2010. Magn. Reson. Imaging 28 (2), 153–162.
Merzouk, S., Zine, N., Agouzoul, M., Janan, M.-T., Bausells, J., Teixidor, F., Jaffrezic-Renault, N., Errachid, A., 2014. Sens. Transducers J. 27, 258–263.
Musameh, M., Wang, J., Merkoci, A., Lin, Y., 2002. Electrochem. Commun. 4 (10), 743–746.
Nesakumar, N., Thandavan, K., Sethuraman, S., Krishnan, U.M., Rayappan, J.B.B., 2014. J. Colloid Interface Sci. 414, 90–96.
Nicholson, R.S., Shain, I., 1964. Anal. Chem. 36 (4), 706–723.
Palleschi, G., Mascini, M., Bernardi, L., Zeppilli, P., 1990. Med. Biol. Eng. Comput. 28 (3), B25–B28.
Pereira, A.C., Aguiar, M.R., Kisner, A., Macedo, D.V., Kubota, L.T., 2007. Sens. Actuators B 124 (1), 269–276.
Prieto-Simón, B., Fàbregas, E., 2004. Biosens. Bioelectron. 19 (10), 1131–1138.
Radoi, A., Compagnone, D., Valcarcel, M.A., Placidi, P., Materazzi, S., Moscone, D., Palleschi, G., 2008. Electrochim. Acta 53 (5), 2161–2169.
Rahman, M.M., Shiddiky, M.J.A., Rahman, M.A., Shim, Y.B., 2009. Anal. Biochem. 384 (1), 159–165.
Rassaei, L., Olthuis, W., Tsujimura, S., Sudhölter, E.J.R., Van Den Berg, A., 2013. Anal. Bioanal. Chem. 406 (1), 123–137.
Rotariu, L., Istrate, O.M., Bala, C., 2014. Sens. Actuators B 191, 491–497.
Rotariu, L., Zamfir, L.G., Bala, C., 2012. Anal. Chim. Acta 748, 81–88.
Saleh, F.S., Okajima, T., Kitamura, F., Mao, L., Ohsaka, T., 2011a. Electrochim. Acta 56 (13), 4916–4923.
Saleh, F.S., Rahman, M.R., Okajima, T., Mao, L., Ohsaka, T., 2011b. Bioelectrochem. 80 (2), 121–127.
Santos, A.D.S., Gorton, L., Kubota, L.T., 2002. Electrochim. Acta 47 (20), 3351–3360.
Sartain, F.K., Yang, X., Lowe, C.R., 2006. Anal. Chem. 78 (16), 5664–5670.
Spohn, U., Narasaiah, D., Gorton, L., 1996. Electroanalysis 8 (6), 507–514.
Tessem, M.B., Swanson, M.G., Keshari, K.R., Albers, M.J., Joun, D., Tabatabai, Z.L., Simko, J.P., Shinohara, K., Nelson, S.J., Vigneron, D.B., Gribbestad, I.S., Kurhanewicz, J., 2008. Magn. Reson. Med. 60 (3), 510–516.
Vallés, C., David Núñez, J., Benito, A.M., Maser, W.K., 2012. Carbon 50 (3), 835–844.
Wulkan, R.W., Verwers, R., Neele, M., Mantel, M.J., 2001. Ann. Clin. Biochem. 38 (5), 554–558.
Yoon, H.C., Kim, H.S., 1996. Anal. Chim. Acta 336 (1–3), 57–65.